NASA
Technical
Paper
2248

January 1984

Performance of Computer-Designed Small-Size Multistage Depressed Collectors for a High-Perveance Traveling Wave Tube

Peter Ramins

NASA

NASA
Technical
Paper
2248

1984

Performance of Computer-Designed Small-Size Multistage Depressed Collectors for a High-Perveance Traveling Wave Tube

Peter Ramins

Lewis Research Center
Cleveland, Ohio

NASA
National Aeronautics
and Space Administration

**Scientific and Technical
Information Branch**

1984

Summary

Computer designed axisymmetric 2.4-cm-diameter three-, four-, and five-stage depressed collectors were evaluated in conjunction with an octave bandwidth, high-perveance, and high-electronic-efficiency, gridded-gun traveling wave tube (TWT). Spent-beam refocusing was used to condition the beam for optimum entry into the depressed collectors.

Both the TWT and multistage depressed collector (MDC) efficiencies were measured, as well as the MDC current, dissipated thermal power, and dc input power distributions for the TWT operating both at saturation over its bandwidth and over its full dynamic range.

Relatively high collector efficiencies were obtained, leading to a very substantial improvement in the overall TWT efficiency. In spite of large fixed TWT body losses (due largely to the 6 to 8 percent beam interception), average overall efficiencies of 45 to 47 percent (for three to five collector stages) were obtained at saturation across the 2.5- to 5.5-GHz operating band. For operation below saturation the collector efficiencies improved steadily, leading to reasonable (>20 percent) overall efficiencies as far as 6 dB below saturation.

Introduction

In a joint USAF-NASA program, the Lewis Research Center is conducting a traveling wave tube (TWT) technology improvement program on TWT's for use in electronic countermeasure and communication systems by applying the multistage depressed collector (MDC) and spent-beam refocusing techniques developed at Lewis (refs. 1 and 2). These techniques convert a large part of the kinetic power of the spent electron beam at the TWT output to useful electric power, substantially increasing the overall efficiency. This is of particular significance to air and space applications because the overall efficiency has a direct bearing on the size, weight, and complexity of the prime power, power conditioning, and heat rejection systems.

The refocusing system and MDC designs are produced by combining the analysis of the TWT, the refocusing system, and the MDC. Representative charges are tracked from the radiofrequency (rf) input of the TWT to their collection on the MDC electrodes (ref. 3).

This design procedure has been highly successful when applied to medium perveance and medium electronic efficiency TWT's (ref. 4). Recently, it was successfully applied to an octave-bandwidth, periodic-permanent-magnet-focused, high-perveance and high-electronic efficiency TWT (Varian TWT Model 6336 A1). A comparison of the computed and measured performance of this TWT, operated at saturation, at a single frequency, and with various MDC's is presented in reference 5. The TWT/MDC performance was also evaluated with three-, four-, and five-stage experimentally optimized collectors, with the TWT operated over its full bandwidth and over its full dynamic range. The results of these tests are reported herein.

Symbols[1]

e	electronic charge
I_B	true interception current in forward direction
I_{body}	I_B+I_S
I_{En}	collector current to n^{th} electrode
I_{E0}	backstreaming current to undepressed collector electrode, if any
I_k	cathode current or beam current
I_S	backstreaming current to TWT body
P_{body}	(total rf losses in TWT) + (true beam interception losses)
P'_{body}	P_{body} + (backstreaming power to body)
P_{coll}	total power in spent beam that enters MDC
P_{fund}	rf output power associated with fundamental frequency
P_{hrm}	rf output power resulting from harmonic frequencies
$P_{\text{recovered}}$	defined in fig. 1
P_{rf}	total rf output ($P_{\text{fund}}+P_{\text{hrm}}$)
$\overline{V}$	average potential of intercepted electrons
V_{en}	voltage on the n^{th} electrode (with respect to ground)
V_k	cathode potential (with respect to ground)
η_e	electronic efficiency of TWT

Experimental TWT and MDC Performance Evaluation

To obtain complete and accurate TWT and MDC performance evaluations, it is necessary to determine the final power distribution in the system. This distribution is shown in figure 1 in the form of power-flow and electron-flow diagrams for a TWT with a depressed collector. Part of the initial beam power V_kI_k appears as measured rf output power at the fundamental and (possibly) harmonic frequencies, and part is dissipated by the TWT body as the sum of rf losses in the TWT and intercepted

[1]See also figs. 1 and 2.

beam power in the forward direction. The rest of the beam power enters the collector. Part of this kinetic power is recovered as useful electric power, and part is dissipated as heat on the collector plates. Collector efficiency is defined as $P_{\text{recovered}}/P_{\text{coll}}$.

With a depressed collector, the possibility exists of backstreaming electrons (I_S and I_{EO} in fig. 1(b)) returning significant power to the TWT body. Since any backstreaming produced by the depressed collector must be accounted for in determining efficiency, this backstreaming power must be evaluated and charged against the depressed collector, or exaggerated collector efficiencies will result.

It should be noted that neither P_{coll}, P_{body}, nor true beam interception I_B can be measured directly for a tube operated with an MDC. Without these measured values, the determination of MDC efficiencies requires certain assumptions that can significantly affect the computed collector performance:

(1) Assumption of the circuit losses (rf losses on the rf structure)

(2) Assumption of the true intercepted current in the forward direction

(3) Assumption of the average energy of the intercepted electrons.

With these assumptions P_{coll} can be computed from the equation

$$P_{\text{coll}} = V_k I_k - (\text{circuit losses}) - (I_B \overline{V}) - P_{\text{rf}}$$

as shown in figure 1(b).

However, it has been our experience at Lewis that both the circuit losses and the true beam interception can vary widely, even between TWT's of identical design. The need for making assumptions can be avoided entirely only by first operating the same TWT with a thermally isolated undepressed collector. The power returned to the TWT body by backstreaming electrons (secondaries) from such a collector is negligible. The power flow diagram for a TWT with an undepressed collector is shown in figure 2. The power into the collector P_{coll} can be measured directly, or, alternatively, P_{rf} and P_{body} can be thermally measured, and P_{coll} computed from measured quantities. Since only the total body power P_{body} is needed for the computation of P_{coll}, it can be seen that, with this experimental approach to the computation of collector efficiency, the questions of circuit efficiency, true interception, and the average energy of the intercepted electrons are irrelevant.

Experimental TWT

A schematic of the Varian TWT Model 6336A1 serial number 101 R1 as modified for use in this program is shown in figure 3, and its general characteristics are shown in table I. A refocusing system consisting of two coils has been added, and the TWT is mounted on a 25.4-cm (10-in.) ultrahigh vacuum (UHV) flange. The UHV valve shown was designed to keep the TWT under vacuum during MDC installation and changes, facilitating startup and minimizing cathode activation problems (ref. 6).

This TWT was delivered with an undepressed thermally isolated water-cooled collector mounted on a matching 25.4-cm (10-in.) vacuum flange. This special collector was required for the bench test.

Experimental Arrangement

Bench Test

The purpose of the bench test was to document the performance of the TWT as delivered with an undepressed collector so that any subsequent TWT performance changes, if any, due to the MDC can be determined and so that accurate MDC efficiency measurements could later be made. The rf load, TWT body, and collector are all thermally isolated and water cooled. Thermal power to each is measured by a combination of a flowmeter and a thermopile. Since the collector is undepressed, the power returned to the TWT by any backstreaming electrons is negligible. The measured P_{body} is, therefore, the sum of the total rf losses in the TWT and the interception losses.

Multistage Depressed Collector Tests

In the MDC test setup (fig. 3) the MDC is mounted on a UHV flange which houses the TWT and vacuum valve. Each MDC electrode is thermally and electrically isolated and is water cooled. The spent-beam power recovered by each MDC electrode, as well as the thermal (kinetic) power dissipated on each electrode, was measured. A vacuum feedthrough drives a variable-length spike. Over its range of variability, the length of the spike significantly affects the electric-field distribution within the collector, and its optimum length can be established quickly and easily for each MDC configuration. Since the refocusing coils and pole pieces are outside the vacuum, they can be manipulated and moved over their designed

TABLE I. – GENERAL CHARACTERISTICS OF VARIAN TWT MODEL 6336A1

Frequency, GHz	2.5 to 5.5
Perveance, $A/V^{3/2}$	1.23×10^{-6}
Maximum total rf output power, W	840
Electronic efficiency (maximum)	.26
Cathode voltage, kV	−6.2
Cathode current, A	.60
Focusing	periodic permanent magnet
Gun	gridded type

range of variability while the TWT is operating. Together with variation of the refocusing coil currents, this enables the rapid optimization, within limits, of the refocusing field profile. Once established, this profile can be synthesized with a permanent-magnet refocusing system. For future work, however, Lewis intends to pursue an alternative approach: use the two permanent magnets past the rf output, already in place in many TWT's, for the refocusing system, and trim their strength for optimum beam entry into the MDC. This approach would minimize the total length of the TWT.

A typical experimental collector arrangement is shown in figure 3. This fully demountable mechanical design was chosen for experimental convenience. Separate water cooling and calorimetry of each collector electrode were chosen for diagnositc purposes and for the system's ability to provide information for the eventual thermal design of a conduction-cooled MDC.

A novel data acquisition system was used to optimize collector efficiency under various conditions. This system provides a real-time readout of the recovered power, as any of the system variables are changed while the TWT is operating. These variables are the individual collector stage voltages, the refocusing coil currents and polepiece locations, and the spike length. Maximizing recovered power is identical to maximizing the MDC efficiency. Once the optimum combination of operating conditions is found, an automated system is used for actual data taking.

Experimental Conditions and Results

RF Test Conditions

Filtered input drive was used at all frequencies. Saturation was set using an uncalibrated power meter which measured rf power only at the fundamental frequency. However, only the total rf power dissipated in the water-cooled matched load was measured, and all TWT overall and electronic efficiencies reported here are based on this P_{rf}.

The TWT is rated for continuous-wave operation. However, to insure that the single tube available would survive the extensive test program, it was operated only at a 25- to 50-percent duty cycle, using 1- to 1.5-ms-pulses. The thermal measurements made were averages over the pulse time, while the electrical measurements (currents) were "instantaneous" samples near the end of the pulse.

Traveling-Wave Tube Bench Test

The TWT, equipped with an undepressed collector, was operated at saturation across the full bandwidth. In addition, at selected operating frequencies, the TWT performance and fixed-body losses were evaluated at rf power levels as much as 15 dB below saturated output power. The results are shown in figures 4 and 5. The fixed TWT losses are a substantial fraction of the rf output power and significantly limit the improvement in overall efficiency obtainable with a depressed collector. Intercepted beam current was in the range of 5.8 to 8.2 (average of 7) percent of I_k across the operating band at saturation and is largely responsible for the large fixed TWT body losses.

After completion of the bench test, the UHV valve (see fig. 3) was closed, and the undepressed collector removed. The TWT was kept under a hard vacuum during the subsequent MDC installations, and no processing (gradual outgassing) of the TWT was required when it was again operated.

Multistage Depressed Collector Test Program

The TWT was operated with a series of MDC's. Some of the results of this optimization program are reported in reference 5. The best results, however, were obtained with experimentally optimized, small extrapolations of the designs reported in reference 5. These three-, four-, and five-stage collectors are shown in figures 6 to 8. None of these collectors used a separate electrode at ground potential. The number of MDC stages is defined as the number of distinct voltages (other than ground potential) needed to operate the MDC. The three- and four-stage collectors are of identical electrode geometry (except for spike length), and their performances were evaluated in a single test.

A coating of carbon black was used to suppress secondary electron emission from the MDC collecting surfaces.

For each design MDC performance was experimentally optimized for the TWT operating at saturation, at the operating frequency corresponding to the highest TWT electronic efficiency (4.75 GHz). This operating point was selected because it usually minimizes the maximum amount of dc input power needed to operate the TWT. Data were then obtained (at this fixed set of refocusing system and MDC operating conditions) across the operating band at saturation and over the full dynamic range of the TWT at 4.75 GHz.

Multistage Depressed Collector Test Results

TWT-MDC Performance Versus Number of Collector Stages at Saturation

The overall TWT efficiency, MDC efficiency, and total DC input power as functions of frequency are shown in

figures 9 to 11 respectively, for the TWT operating at saturation. The results are summarized in table II.

Each of the collectors produced a very substantial improvement in the overall efficiency of the TWT, compared with a single undepressed collector. However, the overall efficiencies obtained were significantly limited by the large fixed TWT losses (6 to 8 percent beam interception).

Each additional collector stage (beyond three) produced only a relatively small improvement. In the case of the five-stage collector, this was due in part to the very limited effort devoted to optimizing the MDC geometry. In the case of the four-stage collector (which was extensively optimized), it turned out that the optimum voltages on two of the lower stages were only 600 V apart, possibly due to a peculiar shape in the spent-beam energy distribution curve. Therefore, these stages could be operated at an optimum single intermediate voltage with only a small reduction in efficiency.

As discussed by Kosmahl (refs. 4 and 7), the collector efficiency (for a given MDC size and number of stages) is a function of the TWT perveance and electronic efficiency. The present results (as well as previous work with other TWT's) support the computed trend shown in figure 7 of reference 4. The 78 percent efficiency obtained with the four-stage collector is close to what may reasonably be expected with this high perveance TWT and is equivalent (in terms of quality) to the mid-80's collector efficiencies that were reported in reference 8 for a 0.4- to 0.5-microperveance and medium electronic efficiency dual-mode TWT.

Collector Current, Dissipated Power, and dc Input Power Distributions at Saturation

The collector current, dissipated thermal power, and dc input power distributions for the three-stage collector are shown in figures 12 to 14 as functions of operating frequency. The corresponding distributions for the four-stage collector are shown in figures 15 to 17; and those for the five-stage collector are shown in figures 18 to 20.

The collector voltages, with respect to ground and normalized to V_k, were as follows:

Collector stage number	Three-stage normalized voltage	Four-stage normalized voltage	Five-stage normalized voltage
1	0.45	0.43	0.43
2	.84	.52	.52
3	1.0	.86	.79
4	----	1.0	.89
5	----	----	1.0

TWT-MDC Performance Versus Number of Collector Stages Over TWT Dynamic Range

The overall TWT efficiency, MDC efficiency, and DC input power as functions of the rf output power level at 4.75 GHz are shown in figures 21 to 23. The MDC operating conditions were identical to those used for saturation. For each of the collectors, MDC efficiency rose steadily (but slowly) for TWT operation increasingly below saturation; and, a reasonable overall efficiency (>20 percent) could be maintained for TWT operation as far as 6 dB below saturation. The collector efficiencies, for each of the collectors, for operation of the TWT in the low end of the linear range was severely limited by the potential (optimized for saturation) of the second most depressed stage. No attempt was made to optimize these collectors for linear operation of the TWT.

Collector Current, Dissipated Power, and dc Input Power Distributions Over TWT Dynamic Range

The collector current, dissipated thermal power, and dc input power distributions for the three-stage collector are shown in figures 24 to 26 as functions of the rf output power level. The corresponding distributions for the four-stage collector are shown in figures 27 to 29; and, those for the five-stage collector are shown in figures 30 to 32. For all of the collectors the maximum value of the current collected by, the thermal power dissipated on,

TABLE II. – SUMMARY OF TWT AND MDC[a] PERFORMANCE AT SATURATION

Number of MDC stages	Overall efficiency at optimization point[b], percent	Collector efficiency at optimization point[b], percent	Maximum dc input power, W	Average overall efficiency[c], percent	Average collector efficiency[c], percent
3	47.2	75.3	1787	44.7	74.4
4	49.0	78.0	1718	46.2	76.7
5	49.9	79.3	1687	47.0	77.9

[a]Active size, 2.4 cm i.d. by 2.8 cm high.

[b]4.75 GHz, saturation; $\eta_e = 0.26$

[c]At 2.5 to 5.5 GHz.

and the dc input power supplied to one or more of the collector stages occurred at the low end of the linear range. Visual observation indicated that the carbon black coating on the second most depressed stage was running red to white hot, particularly at the low end of the linear range. Most of the heat dissipated on the most depressed stage was due to thermal radiation from the next electrode.

Concluding Remarks

Computer designed, small (2.4 cm i.d. by 2.8 cm) three-, four-, and five-stage depressed collectors were optimized and evaluated for an octave bandwidth, high perveance, and high electronic efficiency, gridded-gun TWT. Spent-beam refocusing was used to condition the beam for optimum entry into the depressed collectors.

The MDC efficiencies obtained were very high, considering the high perveance and high electronic efficiency of the TWT and the small size of the collectors. Each of the collectors produced a very substantial improvement in the overall TWT efficiency. Each additional collector stage, however, produced only a modest improvement in performance.

The average overall TWT efficiencies of 45 to 47 percent (for three to five stages) at saturation across the 2.5- to 5.5-GHz operating band were significantly limited by the large fixed body losses of the gridded-gun TWT. For operation of the TWT below saturation, the collector efficiencies were found to improve steadily, leading to reasonable overall TWT efficiencies as far as 6 dB below saturation. This may be of particular significance to the USAF which has expressed interest in dual-mode applications.

Lewis Research Center
National Aeronautics and Space Administration
Cleveland, Ohio, June 20, 1983

References

1. Kosmahl, H. G.: A Novel, Axisymmetric, Electrostatic Collector for Linear Beam Microwave Tubes. NASA TN D-6093, Feb. 1971.
2. Kosmahl, H. G.: An Electron Beam Controller. U.S. Patent 3,764,850, Oct. 1973.
3. Dayton, J. A., Jr.; et al.: Experimental Verification of a Computational Procedure for the Design of TWT-Refocuser-MDC Systems. IEEE Trans. Electron Devices, vol. ED-28, no. 12, Dec. 1981, pp. 1480-1489.
4. Kosmahl, H. K.: Modern Multistage Depressed Collectors—A Review. Proc. IEEE, vol. 70, no. 11, Nov. 1982, pp. 1325-1334.
5. Dayton, J. A., Jr.; et al.: Experimental Verification of the MDC Design Procedure For High Perveance Helix-Type TWT. NASA TP-2162, 1983.
6. Gilmour, A. S., Jr.: Bakeable UHV Gate Valve for Microwave Tube Experimentation. J. Vac. Sci. Technol., vol. 13, no. 6, Nov.-Dec. 1976, pp. 1199-1201.
7. Kosmahl, H. G.: How to Quickly Predict the Overall TWT and the Multistage Depressed Collector Efficiency. IEEE Trans. Electron Devices, vol. ED-27, no. 3, Mar. 1980, pp. 526-529.
8. Ramins, P.; and Fox, T. A.: Multistage Depressed Collector with Efficiency of 90 to 94 Percent for Operation of a Dual-Mode Traveling Wave Tube in the Linear Region. NASA TP-1670, Apr. 1980.

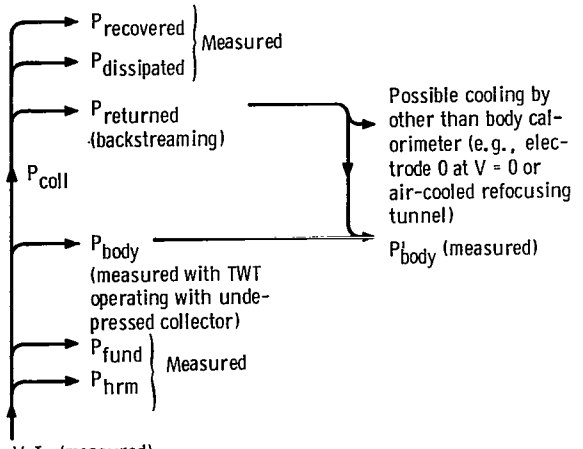

$V_k I_k$ (measured)

P_{body} = (rf circuit losses) + (intercepted power in forward direction)

$P'_{body} = P_{body}$ + (all or part of backstreaming power)

$P_{coll} = V_k I_k - P_{rf} - P_{body}$

Collector efficiency = $P_{recovered}/P_{coll}$

(a)

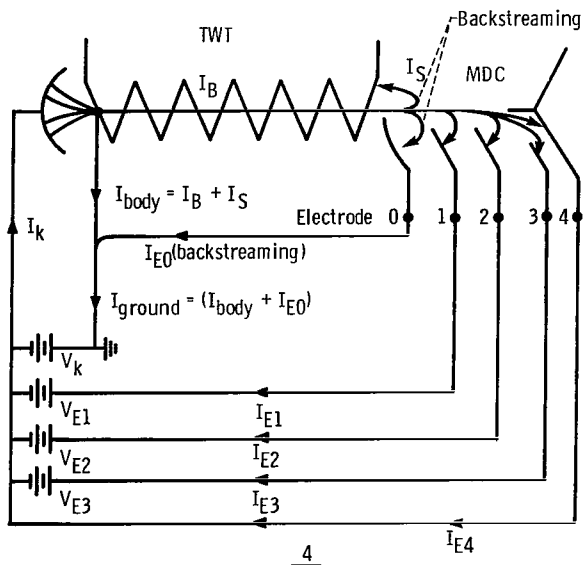

dc input power = $V_k(I_{ground}) + \sum_{n=1}^{4} V_{En} I_{En}$

$$P_{recovered} = \sum_{n=1}^{4} \left(\left| V_k - V_{En} \right| \right) (I_{En})$$

$P_{coll} = V_k I_k - P_{rf}$ - (circuit losses) - $(I_B \bar{V})$, where $\bar{V}$ is average energy of intercepted electrons

$P_{coll} \neq V_k I_k - P_{rf}$ - (circuit losses) - $(I_{ground} V_k)$

(b)

(a) Power flow.
(b) Electron flow.
Figure 1. – Flow diagrams for TWT With MDC.

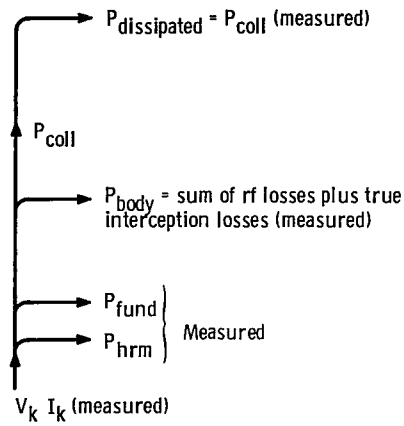

Figure 2. – Power flow for TWT with undepressed collector.

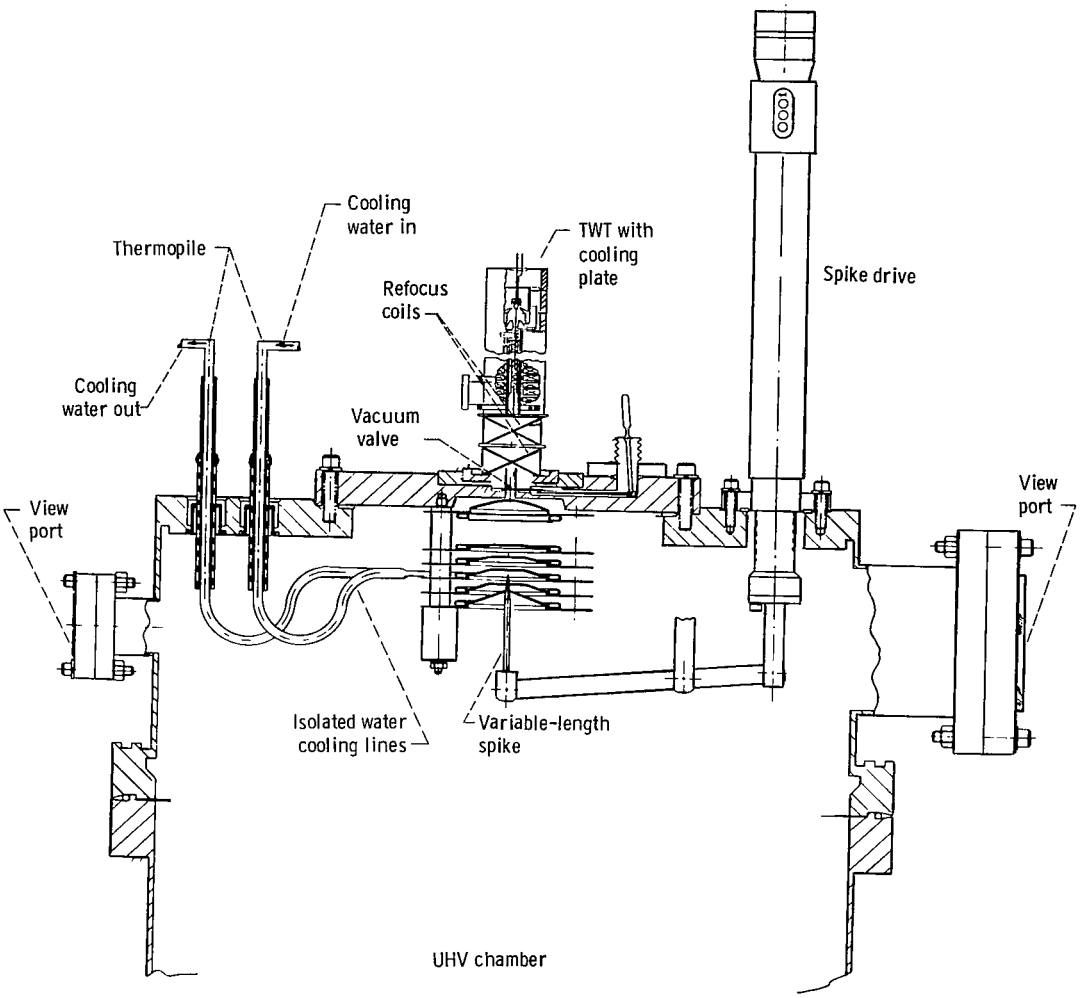

Figure 3. – Schematic of TWT and MDC measuring system.

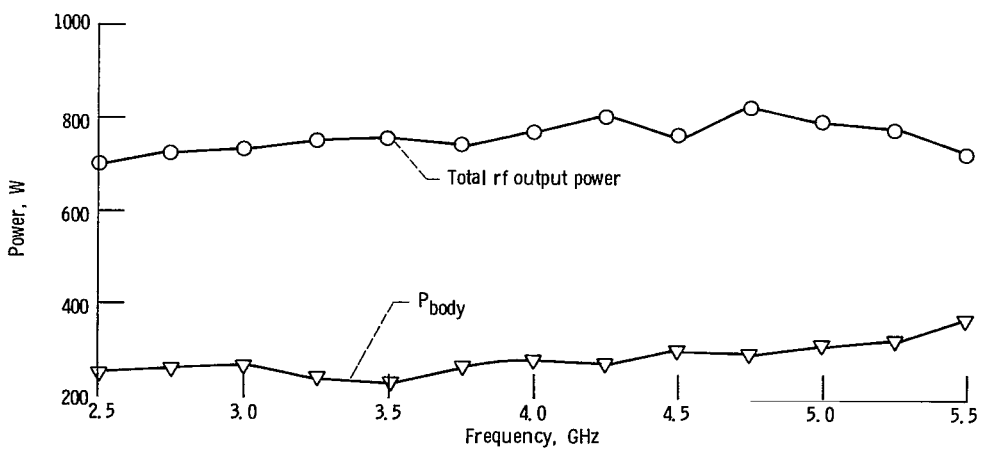

Figure 4. – Radiofrequency power and TWT losses versus frequency at saturation.

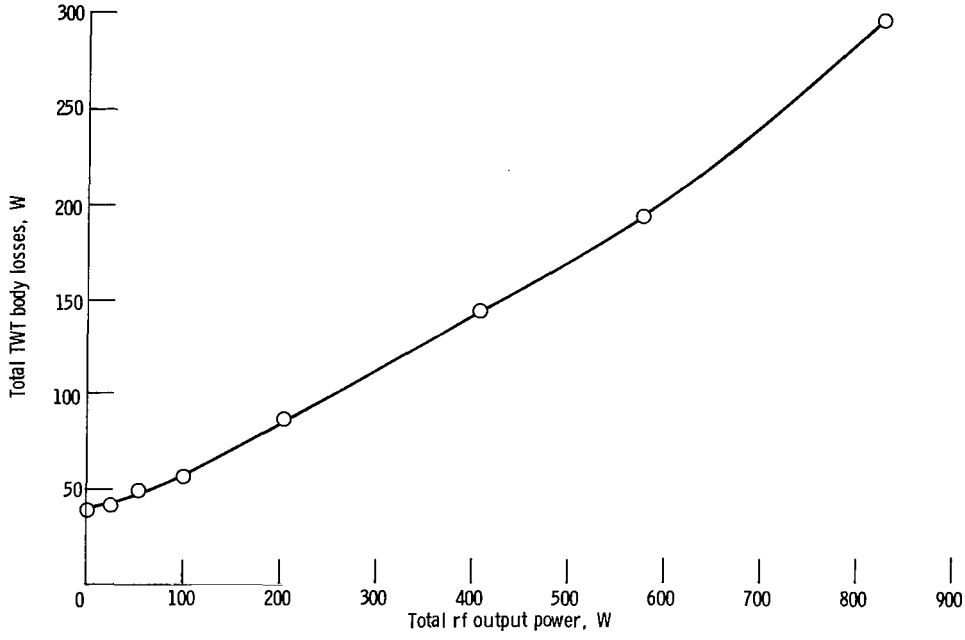

Figure 5. – TWT losses versus total rf output power at 4.75 GHz.

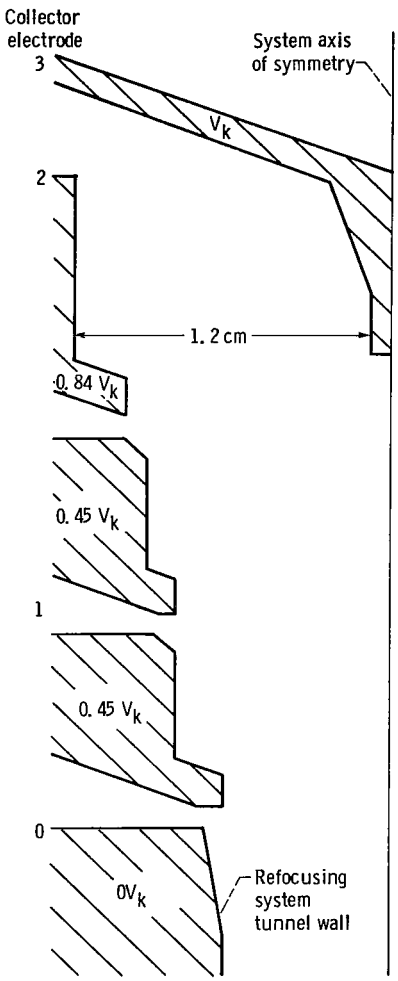

Figure 6. – Three-stage depressed collector geometry and potentials.

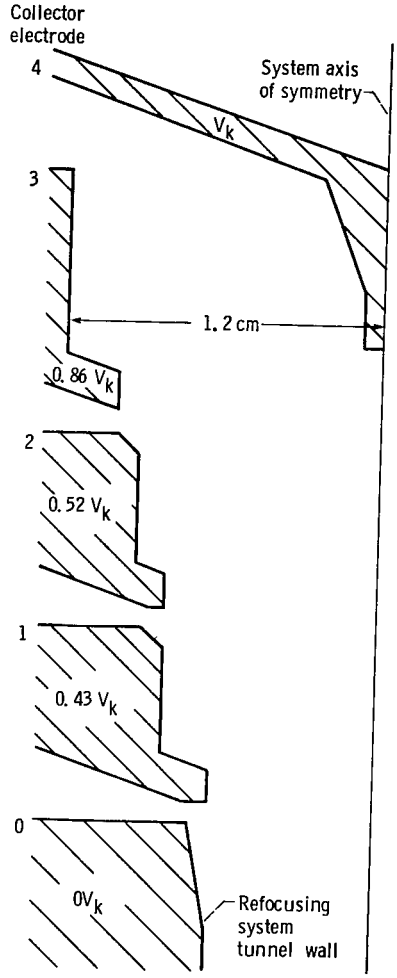

Figure 7. – Four-stage depressed collector geometry and potentials.

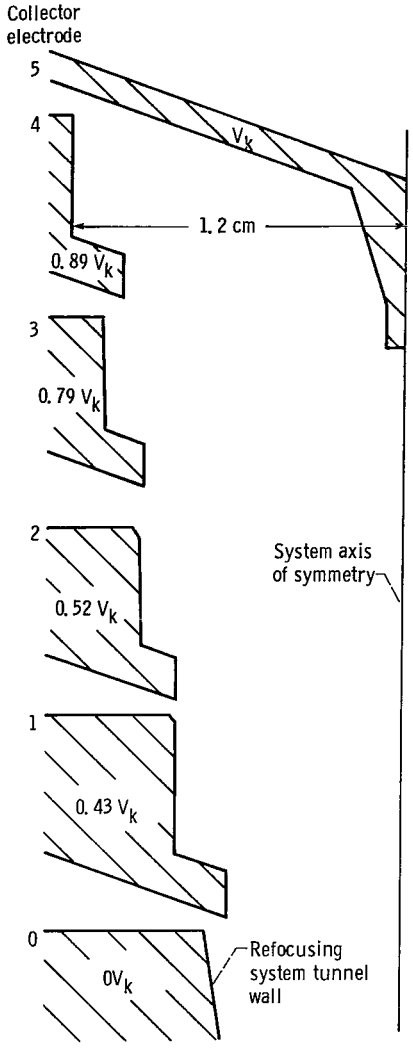

Figure 8. – Five-stage depressed collector geometry and potentials.

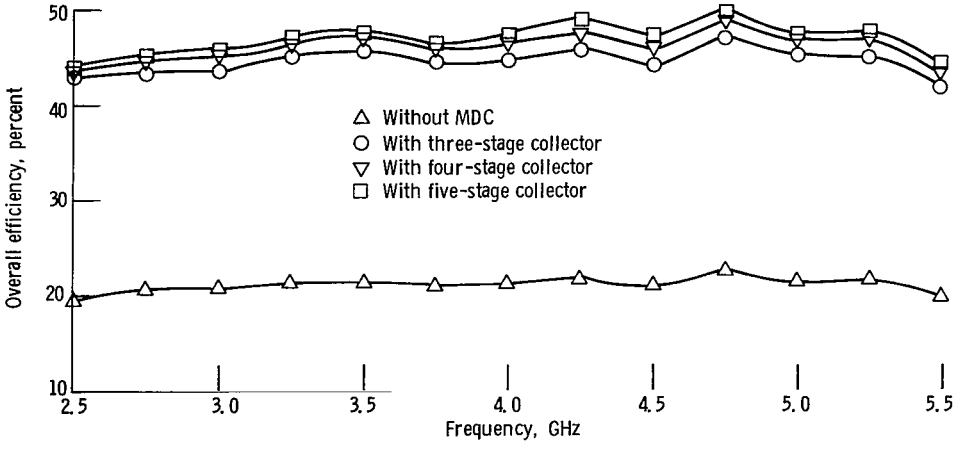

Figure 9. – Overall efficiency versus frequency at saturation.

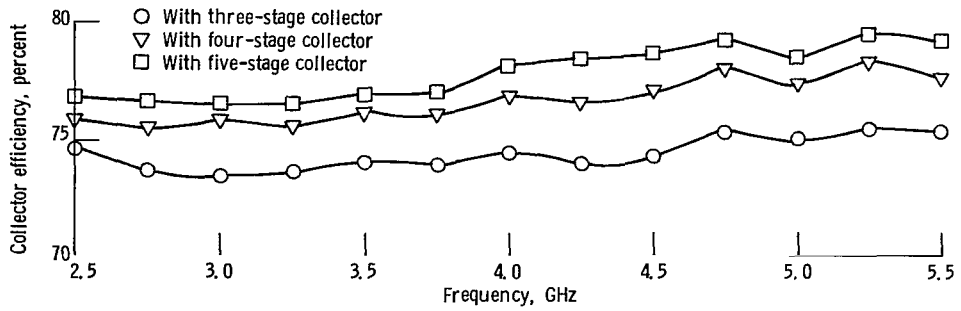

Figure 10. – Collector efficiency versus frequency at saturation.

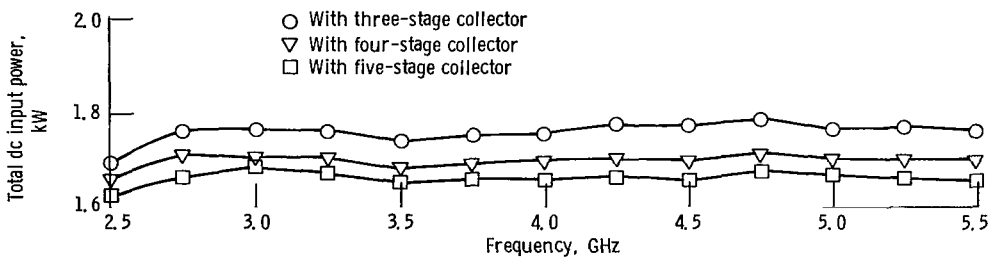

Figure 11. – Total dc input power versus frequency at saturation.

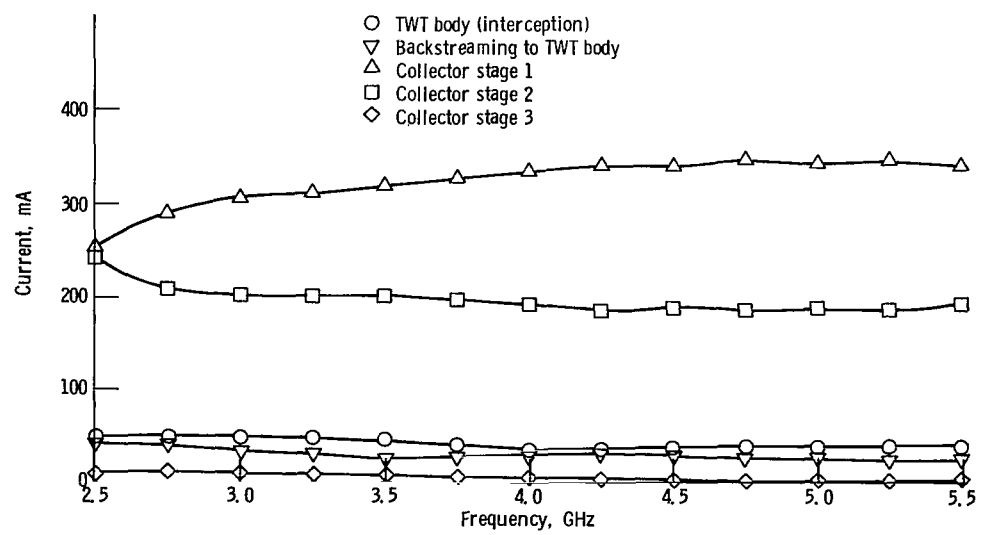

Figure 12. – TWT and three-stage collector currents versus frequency at saturation.

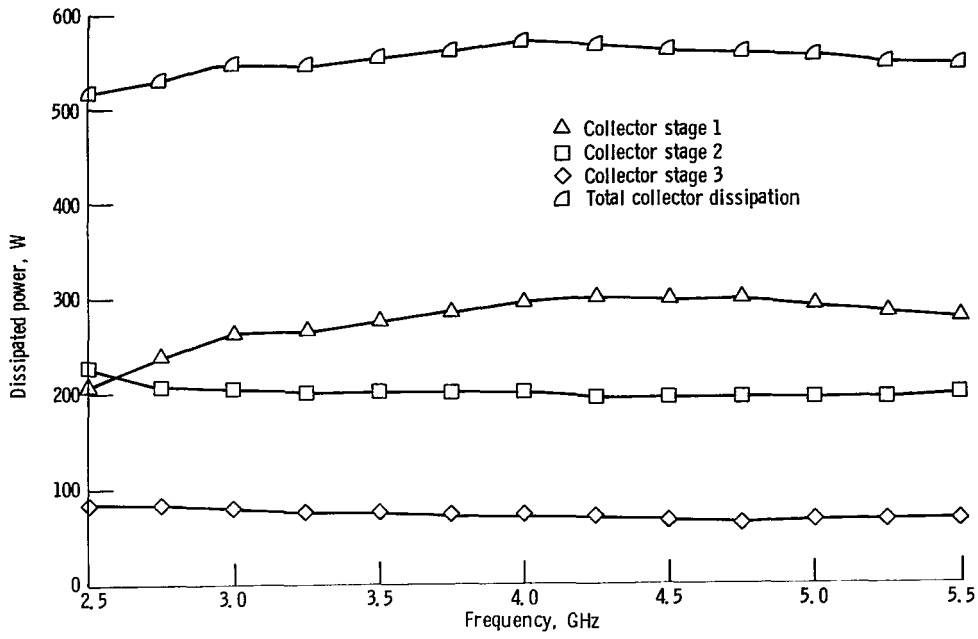

Figure 13. – Thermal power dissipated on three-stage collector electrodes versus frequency at saturation.

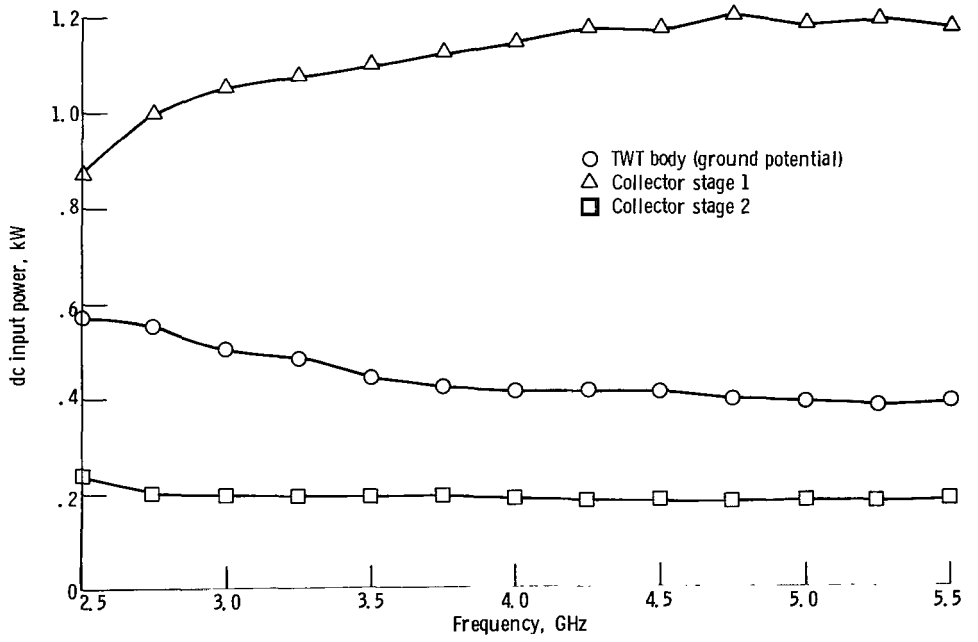

Figure 14. – Direct current input power per electrode in three-stage collector versus frequency at saturation.

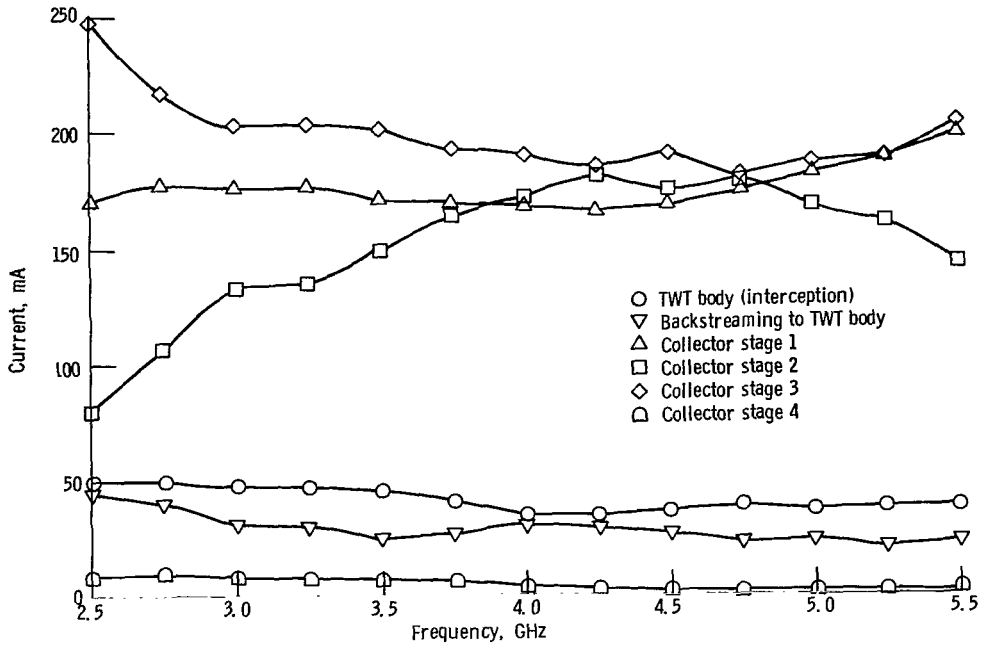

Figure 15. – TWT and four-stage collector currents versus frequency at saturation.

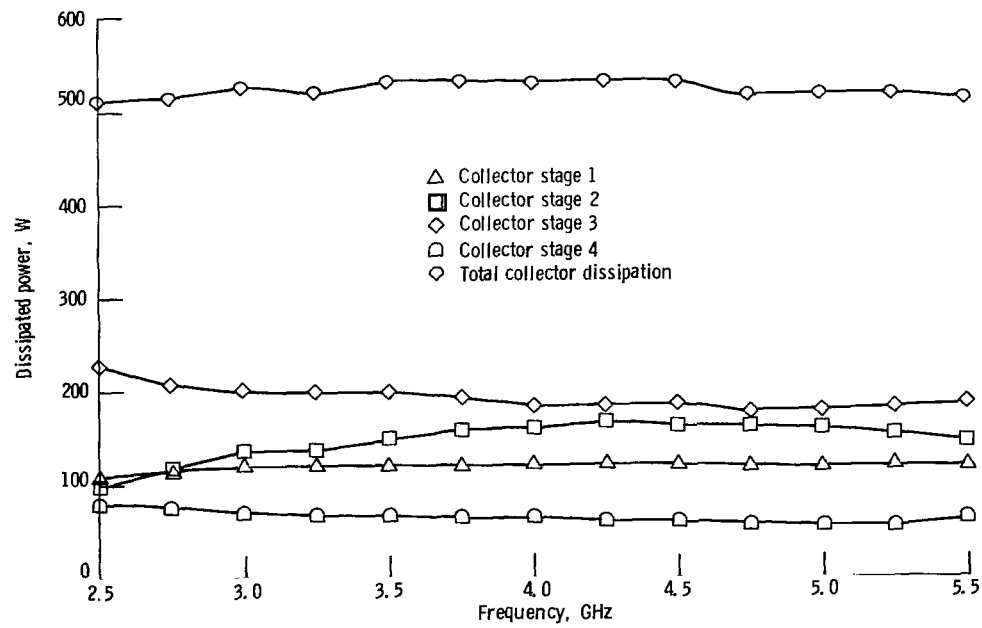

Figure 16. – Thermal power dissipated on four-stage collector electrodes versus frequency at saturation.

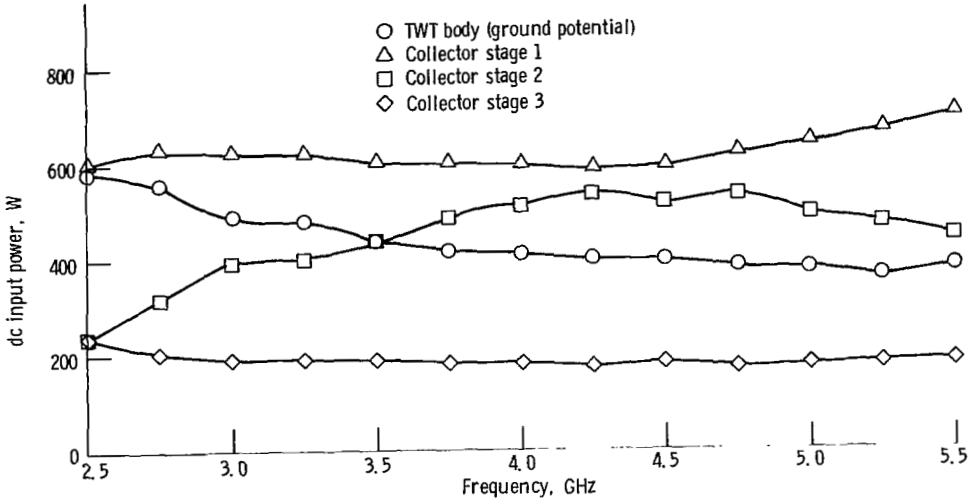

Figure 17. – Direct current input power per electrode in four-stage collector versus frequency at saturation.

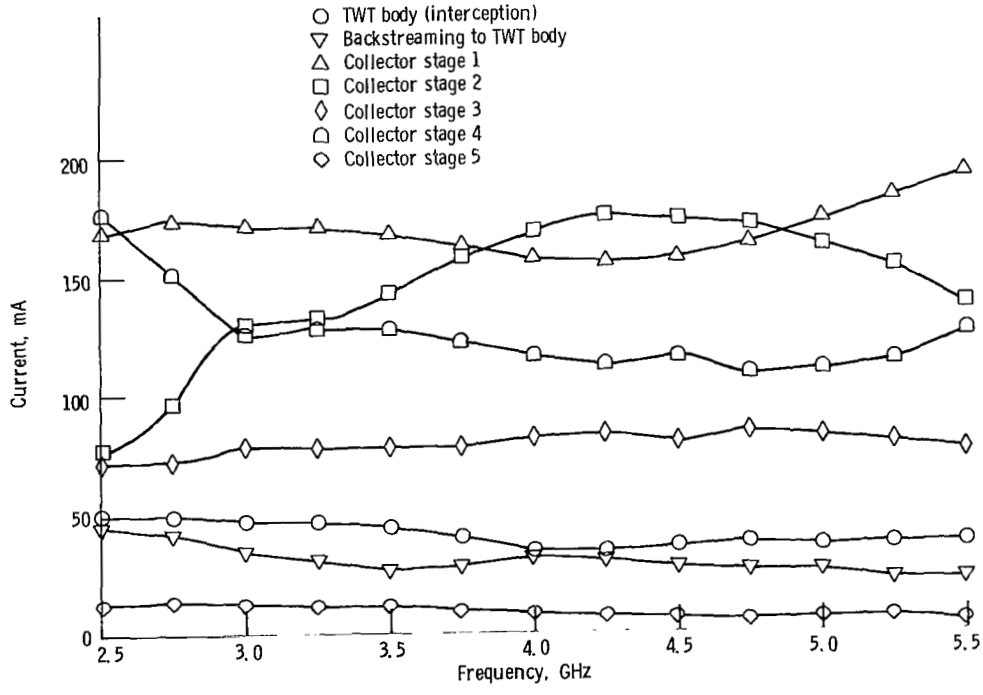

Figure 18. – TWT and five-stage collector currents versus frequency at saturation.

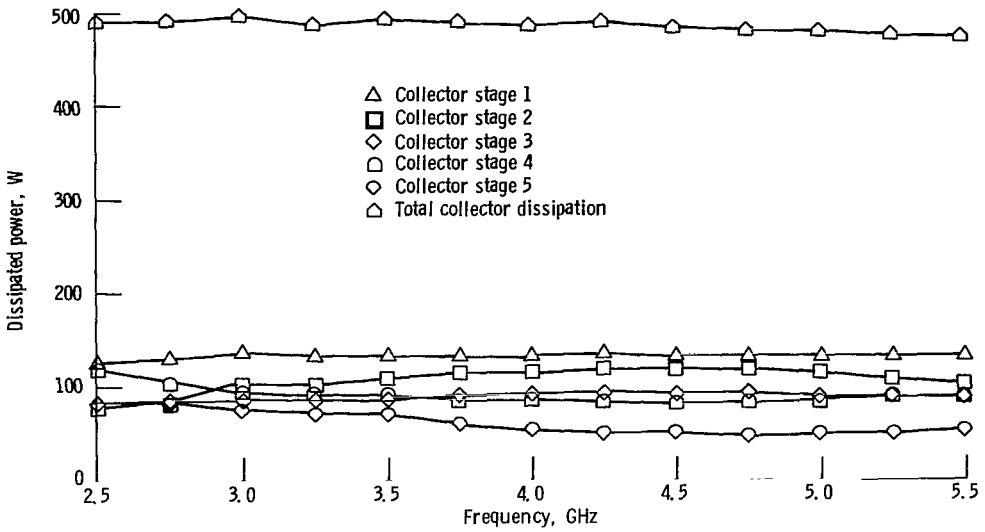

Figure 19. – Thermal power dissipated on five-stage collector electrodes versus frequency at saturation.

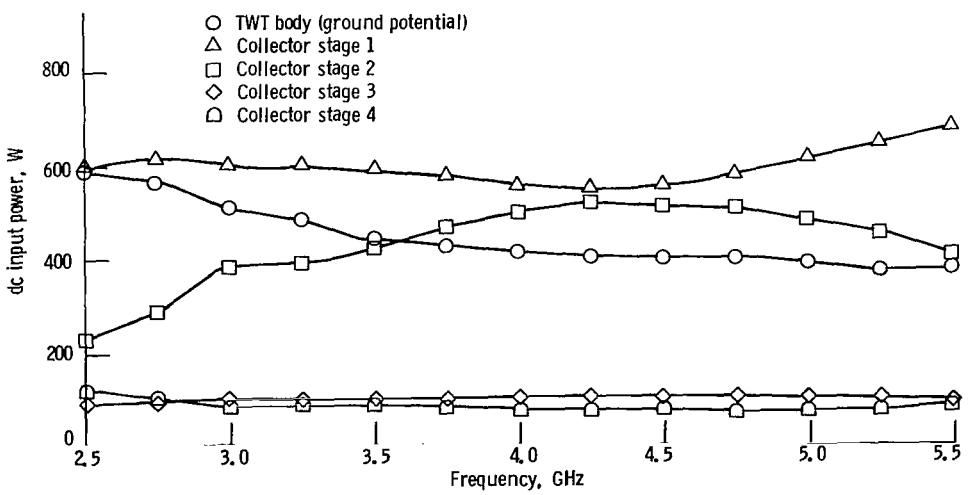

Figure 20. – Direct current input power per electrode in five-stage collector versus frequency at saturation.

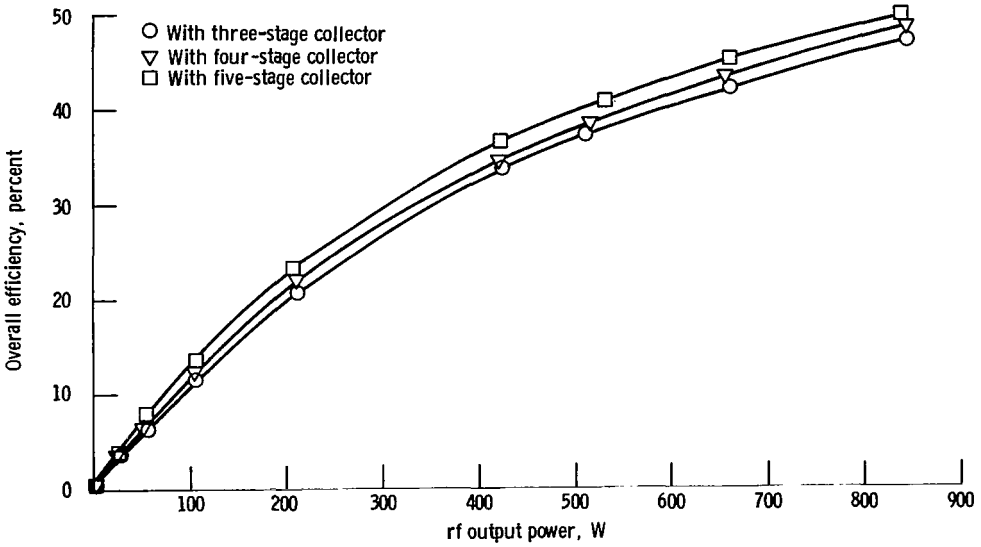

Figure 21. – Overall efficiency versus radiofrequency power at 4.75 GHz.

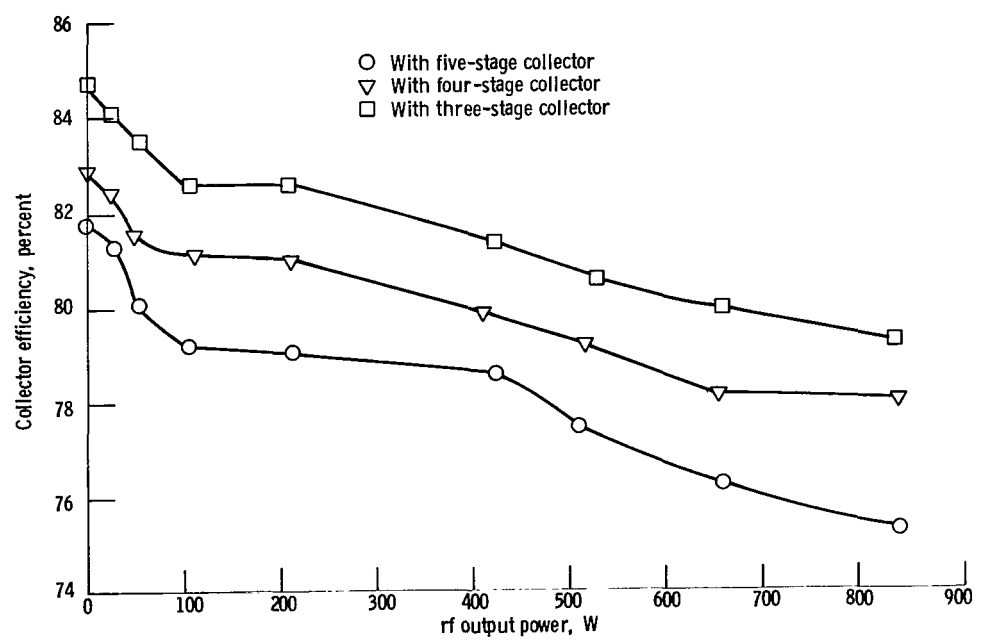

Figure 22. – Collector efficiency versus radiofrequency power at 4.75 GHz.

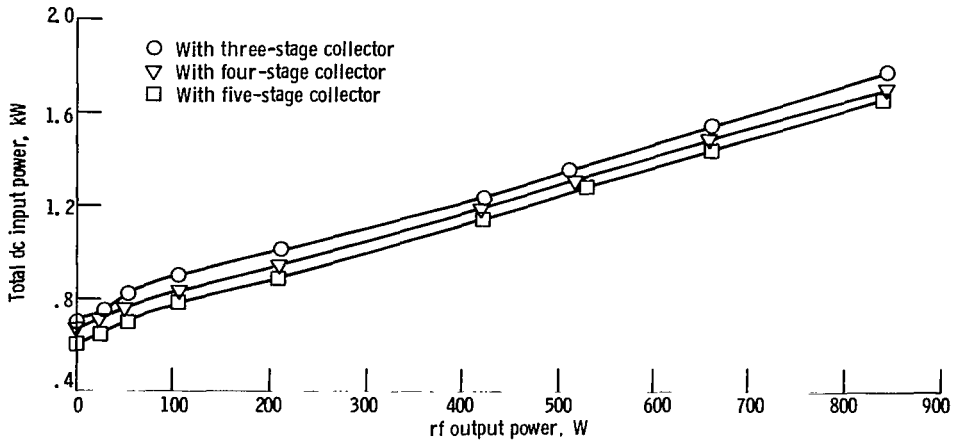

Figure 23. – Total dc input power versus radiofrequency power at 4.75 GHz.

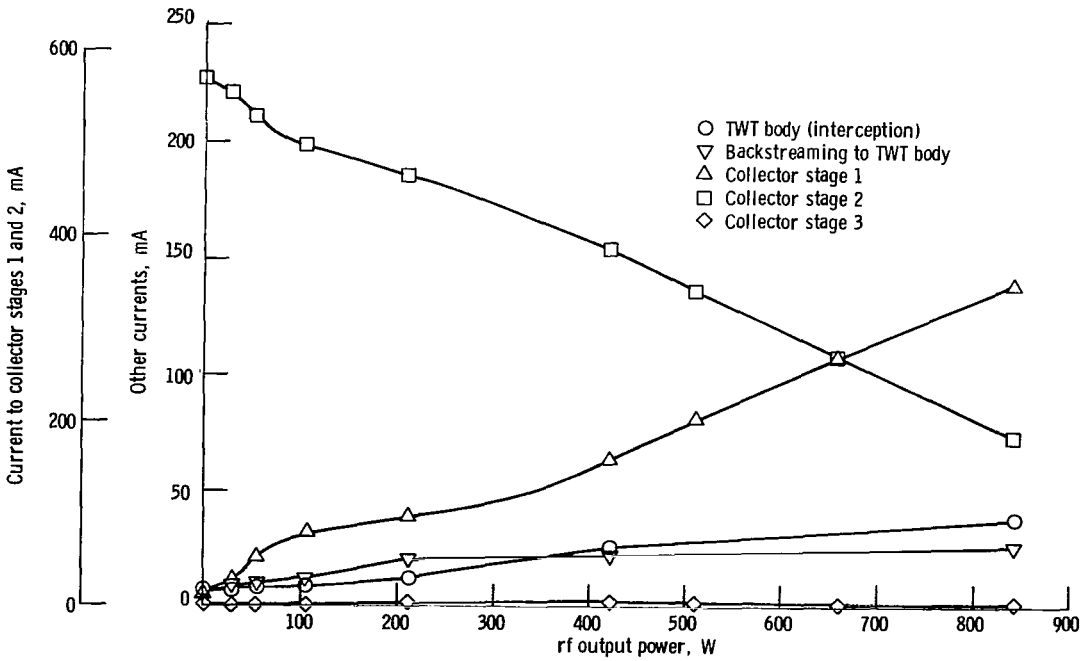

Figure 24. – TWT and three-stage collector currents versus radiofrequency power at 4.75 GHz.

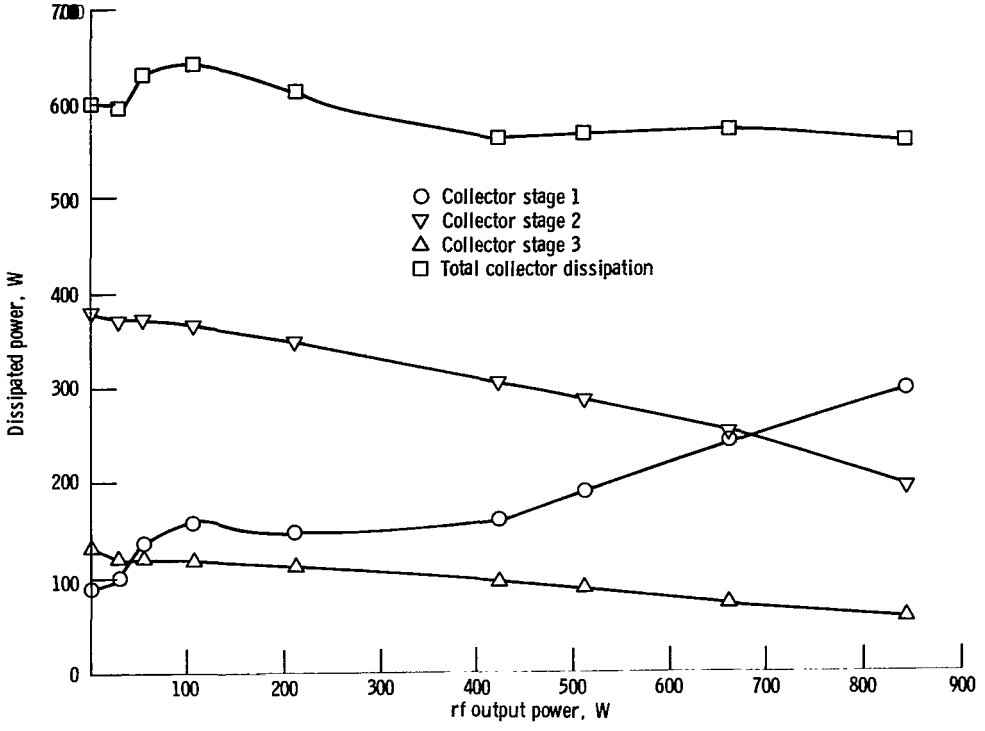

Figure 25. – Thermal power dissipated on three-stage collector electrodes versus radiofrequency power at 4.75 GHz.

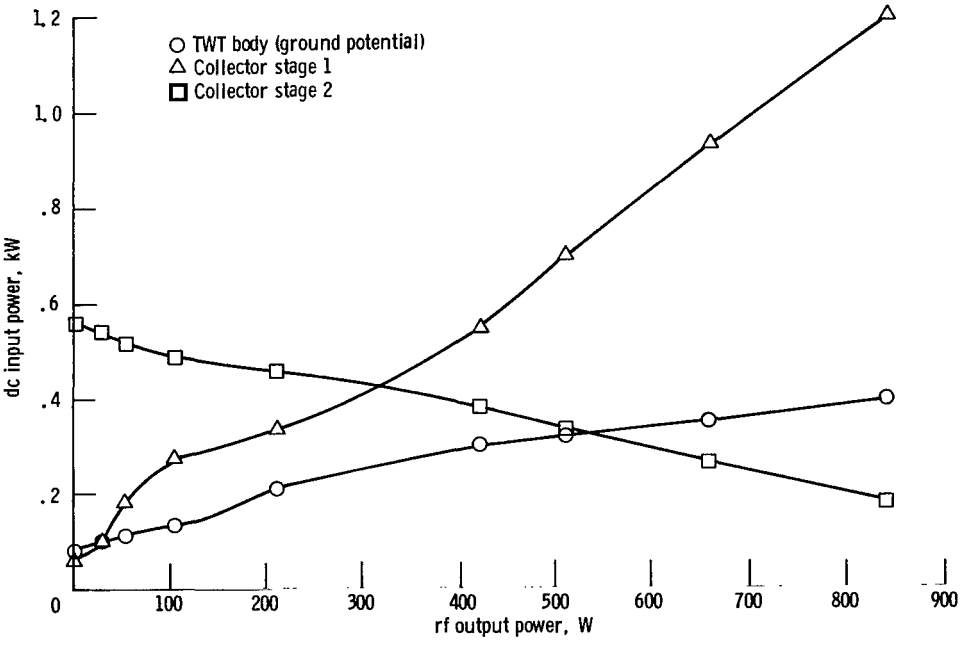

Figure 26. – Direct current input power per electrode in three-stage collector versus radiofrequency power at 4.75 GHz.

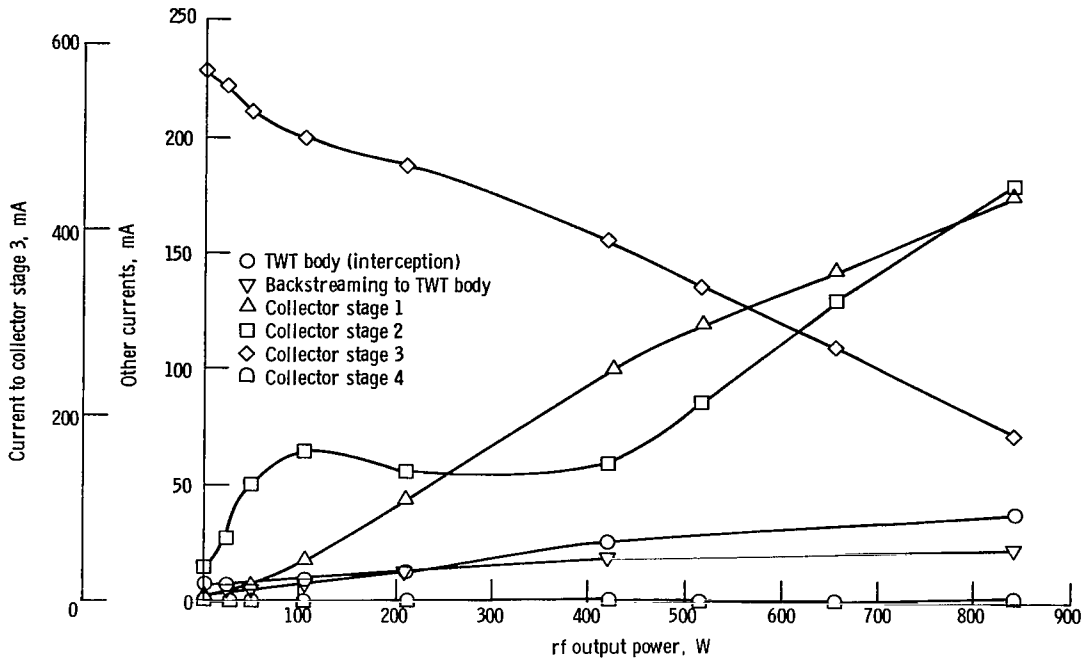

Figure 27. – TWT and four-stage collector currents versus radiofrequency power at 4.75 GHz.

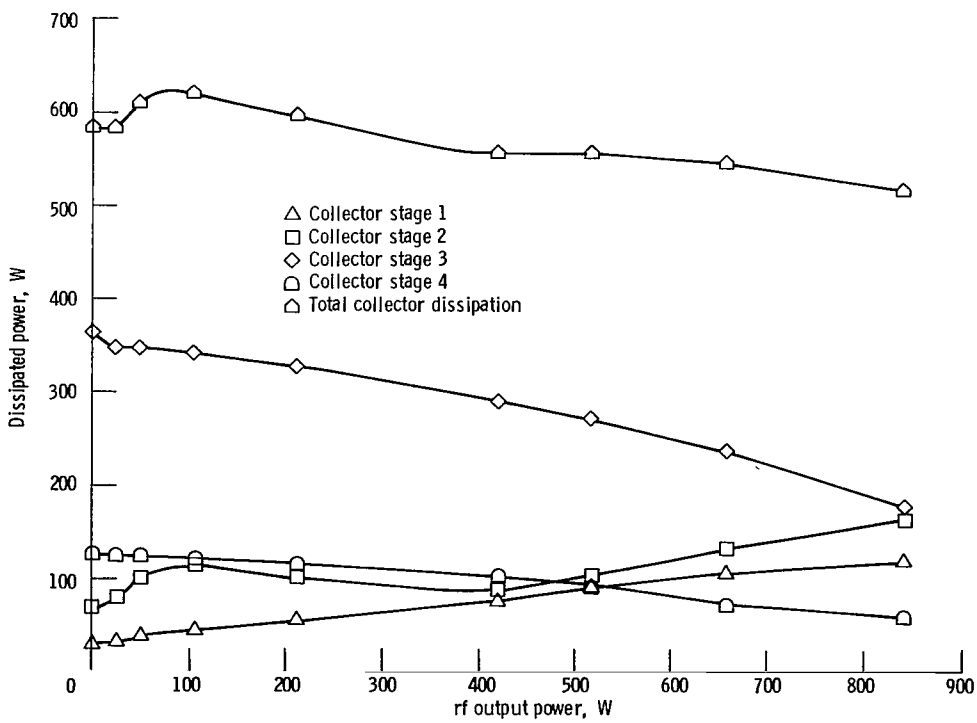

Figure 28. – Thermal power dissipated on four-stage collector electrodes versus radiofrequency power at 4.75 GHz.

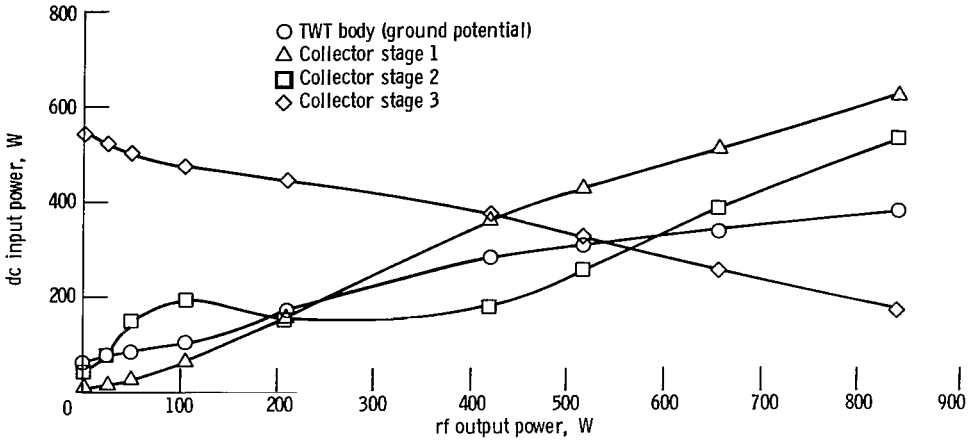

Figure 29. – Direct current input power per electrode in four-stage collector versus radiofrequency power at 4.75 GHz.

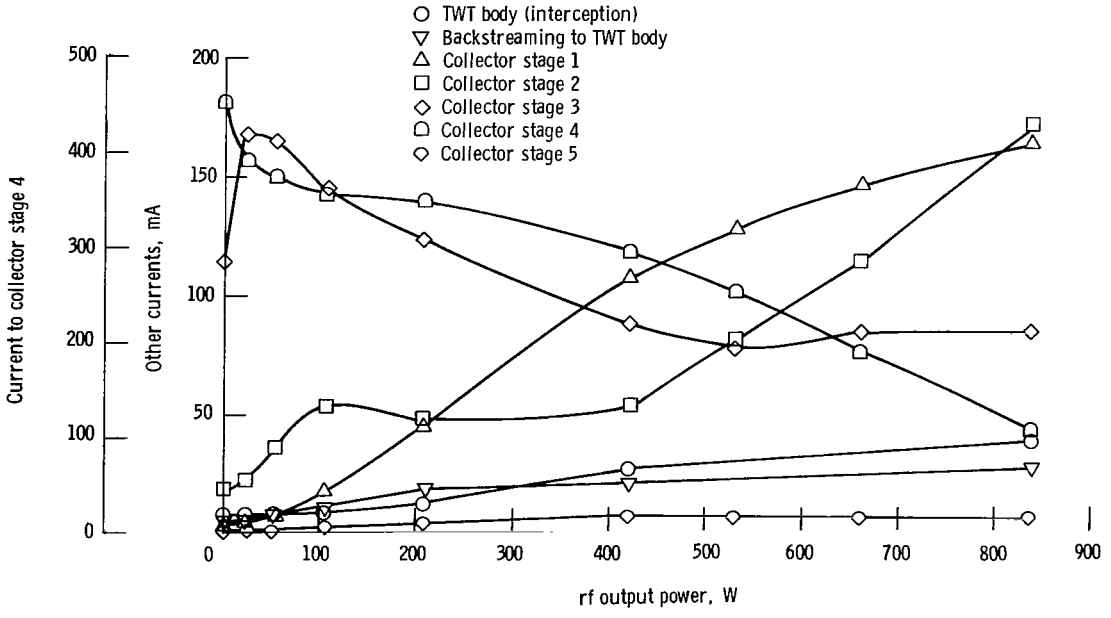

Figure 30. – TWT and five-stage collector currents versus radiofrequency power at 4.75 GHz.

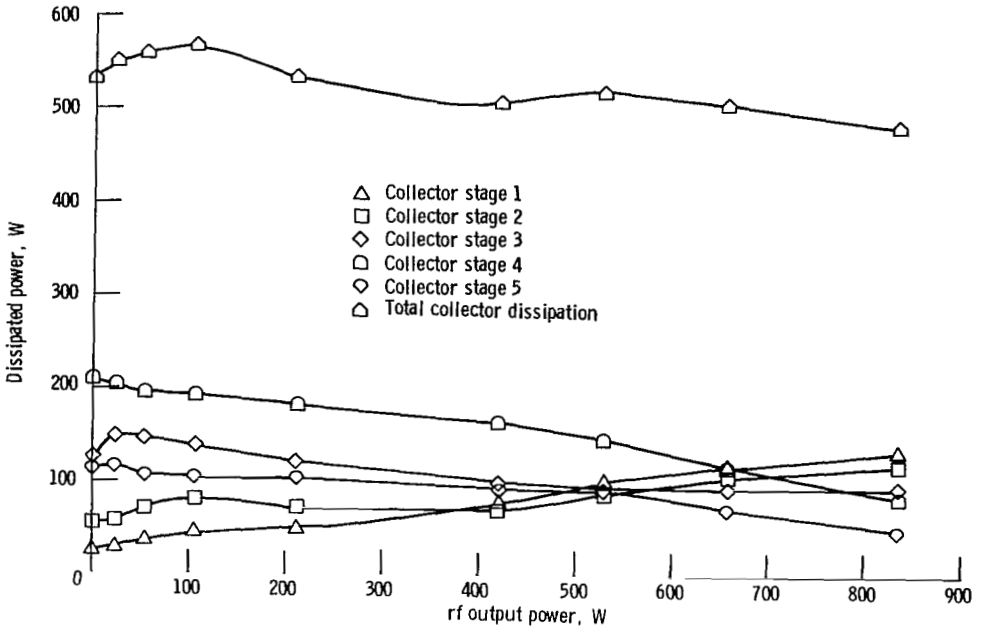

Figure 31. – Thermal power dissipated on five-stage collector electrodes versus radiofrequency power at 4.75 GHz.

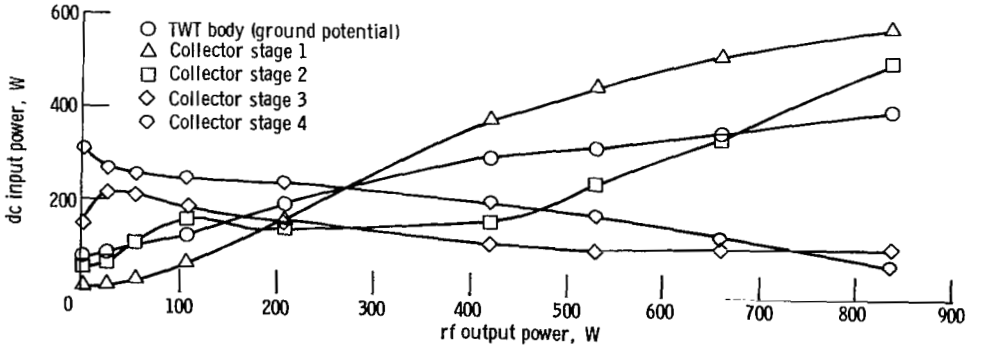

Figure 32. – Direct current input power per electrode in five-stage collector versus radiofrequency power at 4.75 GHz.

1. Report No.	2. Government Accession No.	3. Recipient's Catalog No.
NASA TP-2248		

4. Title and Subtitle
Performance of Computer-Designed Small-Size Multistage Depressed Collectors for a High-Perveance Traveling Wave Tube

5. Report Date
January 1984

6. Performing Organization Code
506-58-22

7. Author(s)
Peter Ramins

8. Performing Organization Report No.
E-1700

10. Work Unit No.

9. Performing Organization Name and Address
National Aeronautics and Space Administration
Lewis Research Center
Cleveland, Ohio 44135

11. Contract or Grant No.

13. Type of Report and Period Covered
Technical Paper

12. Sponsoring Agency Name and Address
National Aeronautics and Space Administration
Washington, D.C. 20546

14. Sponsoring Agency Code

15. Supplementary Notes

16. Abstract

Computer designed axisymmetric 2.4-cm-diameter three-, four-, and five-stage depressed collectors were evaluated in conjunction with an octave bandwidth, high-perveance, and high-electronic-efficiency, gridded-gun traveling wave tube (TWT). Spent-beam refocusing was used to condition the beam for optimum entry into the depressed collectors. Both the TWT and multistage depressed collector (MDC) efficiencies were measured, as well as the MDC current, dissipated thermal power, and dc input power distributions, for the TWT operating both at saturation over its bandwidth and over its full dynamic range. Relatively high collector efficiencies were obtained, leading to a very substantial improvement in the overall TWT efficiency. In spite of large fixed TWT body losses (due largely to the 6 to 8 percent beam interception), average overall efficiencies of 45 to 47 percent (for three to five collector stages) were obtained at saturation across the 2.5-, to 5.5-GHz operating band. For operation below saturation the collector efficiencies improved steadily, leading to reasonable (>20 percent) overall efficiencies as far as 6 dB below saturation.

17. Key Words (Suggested by Author(s))	18. Distribution Statement
Traveling wave tube Multistage depressed collector High efficiency	Unclassified - unlimited STAR Category: 33

19. Security Classif. (of this report)	20. Security Classif. (of this page)	21. No. of pages	22. Price*
Unclassified	Unclassified	22	A02

*For sale by the National Technical Information Service, Springfield, Virginia 22161

NASA-Langley, 1984

National Aeronautics and
Space Administration

Washington, D.C.
20546

Official Business
Penalty for Private Use, $300

THIRD-CLASS BULK RATE

Postage and Fees Paid
National Aeronautics and
Space Administration
NASA-451

U.S.MAIL

4 1 U.D. 831216 S0090305
DEPT OF THE AIR FORCE
AF WEAPONS LABORATORY
ATTN: TECHNICAL LIBRARY (SUL)
KIRTLAND AFB NM 87117

NASA

POSTMASTER: If Undeliverable (Section 158 Postal Manual) Do Not Return